ARTICLE

Photochemically Controlled Synthesis of Anisotropic Au Nanostructures: Platelet-like Au Nanorods and Six-Star Au Nanoparticles

Xiao Huang,[†] Xiaoying Qi,[†] Yizhong Huang,[†] Shaozhou Li,[†] Can Xue,[†] Chee Lip Gan,[†] Freddy Boey,[†,‡] and Hua Zhang*[,†,‡]

[†]School of Materials Science and Engineering, Nanyang Technological University, 50 Nanyang Avenue, Singapore 639798, Singapore, and [‡]Center for Biomimetic Sensor Science, Nanyang Technological University, 50 Nanyang Drive, Singapore 637553

ABSTRACT We report the shape-controlled synthesis of anisotropic Au nanostructures through TiO_2-assisted photochemical reduction of $HAuCl_4$. By using this method, we have successfully synthesized the platelet-like Au nanorods and six-star Au nanoparticles. Importantly, the platelet Au nanorod exhibits the unique asymmetric five-twinned structure. The colloidal TiO_2 sols were used as both the photocatalyst to initiate the reaction and the stabilizing agent for the produced Au nanostructures. Significantly, in this photochemical process, the tunable irradiation intensity allows us to kinetically control the crystal evolution at various growth stages, leading to the shape difference of ultimate gold nanostructures. Our synthetic method shows a great potential as an alternative or supplement to the other wet chemical approaches for the shape-control of metallic nanostructures.

KEYWORDS: Au nanostructures · Au nanorods · Au nanoparticles · photochemical synthesis · shape control

Gold nanoparticles (AuNPs) have been substantially explored and widely used in catalysis, electronics, photonics, and biosensing, *etc.*[1−3] Great efforts have contributed to the synthesis of AuNPs with unique chemical and physical properties that are tunable through the control of size, shape, and crystallinity.[4,5] Anisotropic Au nanostructures, such as nanoplatelets, multipods, nanostars, nanobelts, and nanorods,[6−13] are receiving special attention because of their special properties. For example, the shape and size-directed surface plasmon resonance (SPR) in the visible and near-infrared (IR) range[8,12] renders them useful in wide applications in sensing, imaging, and cancer theropy.[14,15]

The shape control has been the focus of the synthesis of metallic nanocrystals.[9,12,16−20] In general, a symmetry breaking event is to take place to facilitate the anisotropic development.[18−22] Various synthesis methods have been developed to synthesize anisotropic nanostructures, such as the surfactant-directed seed-mediated method,[6] polyol method,[8] templated electrochemical method,[23−25] sonochemical method,[11] photochemical route,[26] soft-templated organic synthesis,[27−29] and especially the recent graphene-templated synthesis.[30] By using these methods, anisotropic Au nanocrystals (AuNCs), such as triangular nanoprisms,[17] nanorods,[13,26] and nanowires,[27−29] were synthesized with good quality control.

As part of efforts toward the green chemistry,[31] the photochemical route has been developed to synthesize the noble metal NPs.[26,32−36] For example, Eustis *et al.* obtained AuNPs from the photochemical reduction of Au^{3+} in the presence of poly(vinylpyrrolidone) (PVP) and ethylene glycol (EG).[33] Wang *et al.* synthesized Au clusters with TiO_2 particles as templates by UV irradiation of the mixture of TiO_2 colloid and Au salt.[34,35] Kim *et al.* reported the synthesis of short Au nanorods with UV irradiation of the aqueous solution containing $HAuCl_4$, cetyl trimethylammonium bromide (CTAB), and Ag ions.[26] However, all the aforementioned photochemical methods have not given good controllability over the shape and size of the synthesized Au nanostructures, compared with the surfactant-assisted seed-mediated chemical reduction[6] and the polyol approach.[8] Herein, we developed a facile method to synthesize anisotropic AuNCs with controlled morphologies by photoirradiation of an ethanolic solution containing $HAuCl_4$ and TiO_2 sols without the addition of any other surface capping molecules. By simply varying the concentrations of $HAuCl_4$ and TiO_2, and adjusting the

*Address correspondence to hzhang@ntu.edu.sg, hzhang166@yahoo.com.

Received for review July 28, 2010 and accepted September 21, 2010.

Published online October 6, 2010. 10.1021/nn101803m

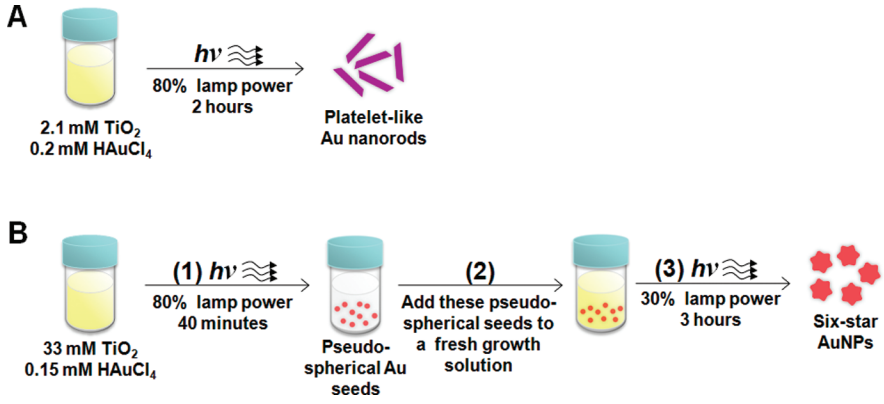

Scheme 1. Schematic illustration of the TiO_2-catalyzed photochemical synthesis of (A) Au platelet-like nanorods and (B) six-star AuNPs.

power of the light source at different reaction stages. AuNCs with different morphologies were synthesized. Two unique structures obtained in our experiment, namely, platelet-like Au nanorods, and six-star AuNPs, were investigated in detail by using scanning electron microscopy (SEM), transmission electron microscopy (TEM), and geometric phase analysis (GPA). The growth mechanism in the shape-controlled photochemical synthesis is also discussed.

RESULTS AND DISCUSSION

Synthesis and Characterization of Platelet-like Au Nanorods. Scheme 1A shows how to synthesize the Au platelet-like nanorods. When the mixed ethanolic solution of $HAuCl_4$ (*ca.* 0.2 mM) and TiO_2 sol (*ca.* 2.1 mM) was photoirradiated by a 150 W halogen lamp (at 80% of the lamp power) for 2 h, the platelet-like Au nanorods were synthesized. The length of these Au nanorods is 1.3 ± 0.3 μm, and the width is 66.7 ± 7.5 nm (Figure 1A). The inset SEM image in Figure 1A reveals the tip morphology of such an Au nanorod. The top and bottom planes are parallel to each other, and the thickness is about 30 nm. Interestingly, if viewed along its basal plane, both ends of the rod are terminated by tips with the interplane angles of 60° as shown in Figure 1B, 1D and Figure S1 in Supporting Information (SI). These nanorods are different from the commonly synthesized Au nanorods with pentagonal cross sections,[13] or the Au nanobelts having a rectangular tip morphology.[11] The SAED pattern taken on a typical Au nanorod with the electron beam posed normal to its basal plane shows a superposition of two specific crystallographic zones, that is, the ⟨111⟩ and ⟨110⟩ zones (Figure 1C), indicating a mixture of crystal domains.[21] Reflections of planes $(0\bar{2}2)$, (202), and (220) of the ⟨111⟩ zone, and $(\bar{1}\bar{1}\bar{1})$, $(11\bar{3})$, $(22\bar{2})$, and (220) of the ⟨110⟩ zone are labeled in Figure 1C. The two crystallographic zones share a common reflection of (220), corresponding to the [110] direction of the rod's elongation. To further understand the crystal structure of the platelet Au nanorods, the focused ion beam (FIB) was used to cut a typical rod, which was then mounted on a copper grid for TEM analysis. Although the platelet-like Au nanorod also contains the 5-fold twins (Figure 1E, five twin domains are numbered as T1−T5),[13,14] surprisingly, one of the twin boundaries (*i.e.*, the boundary of T2 and T3, inset of Figure 1E) is longer than the others, which is different from the Au nanorods with symmetric pentagonal cross sections.[13] This distortion results in the generation of two parallel {111} planes, that is, the top and bottom basal planes of the platelet rod (Figure 1E−G). HRTEM image of the rod's cross-section (Figure 1F) and the fast Fourier transform (FFT) generated selective area electron diffraction (SAED) pattern (Figure 1G) further confirm the five-twined nature of the synthesized Au nanorods. Two families of planes with lattice spacings of 2.0 and 2.4 Å are measured in each domain, corresponding to the (200) and (111) planes

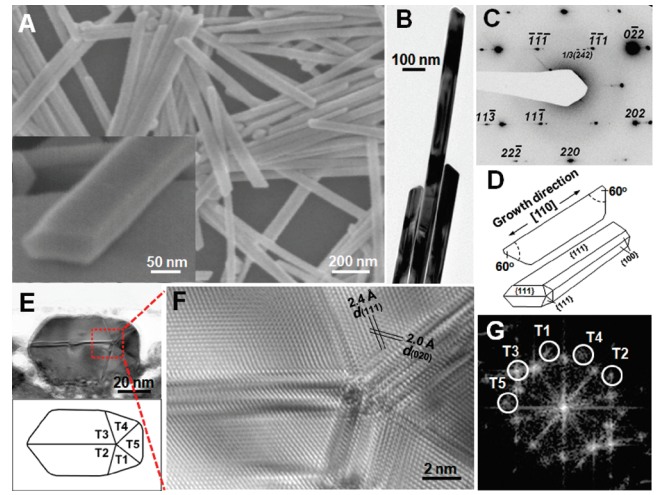

Figure 1. (A) SEM image of Au platelet-like nanorods. Inset: magnified SEM image of the tip portion of a typical nanorod. (B) TEM image of three nanorods with even widths and similar tip morphologies. (C) SAED pattern of an Au nanorod with its wider basal plane normal to the electron beam. (D) Crystallographic model of an Au nanorod. (E) TEM image of the cross-section of a typical Au nanorod, prepared by focused ion beam (FIB). Inset: schematic illustration of the 5-fold twinned cross-section. (F) HRTEM image of the designated area in panel E. (G) Fast Fourier transform (FFT) generated diffraction pattern of panel F.

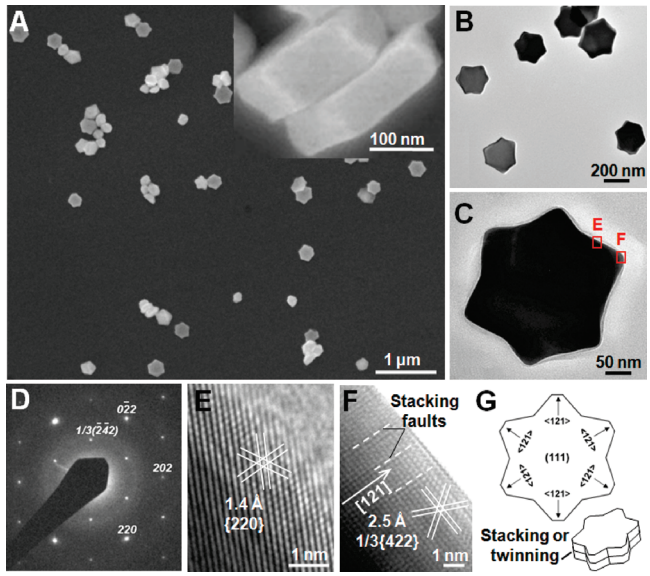

Figure 2. (A) SEM image of star-shaped AuNPs. Inset: side view of two six-star AuNPs. (B) TEM image of star-shaped AuNPs. (C) TEM image of a typical six-star AuNP. (D) SAED pattern of a six-star AuNP along the [111] zone axis. (E and F) HRTEM images of the edge and the tip of a six-star NP designated in panel C. (G) A crystallographic model of a six-star AuNP.

(Figure 1F), respectively, with [110] as the common zone axis (Figure 1G, the (002) diffraction spot for each domain is highlighted in the white circle).[13] Note that the 5-fold axis is not at the geometric center of the rod's cross section.[37,38] The formation of such asymmetrically 5-fold twinned Au nanorods can be explained, in part, by the tendency to minimize surface energy during crystal growth. It is known that fcc Au nanostructures are commonly bound by mixed low index planes, that is, the (110), (100), and (111) planes, and the surface energies for them are in the order of $\gamma_{(110)} > \gamma_{(100)} > \gamma_{(111)}$.[20] Therefore, driven by thermodynamics, the structures tend to maximize the facets enclosed by the {111} planes. Evidently, in a platelet-like Au nanorod, the asymmetric 5-fold twinning gives rise to two additional {111} planes as the top and bottom basal planes of the nanorod (Figure 1D−E). This is in contrast to the nanorods (or nanowires) with symmetric pentagonal cross sections, grown in the CTAB-assisted seed-mediated method and mainly covered by the {100} side planes.[13,14] In that case, CTAB double-layers preferentially absorb on the {100} planes compared to the {111} planes, which kinetically decrease the surface energies.[14] A schematic crystal model is thus proposed in Figure 1D. The platelet-like nanorod exhibits the asymmetric 5-fold twins. The nanorod is bound by mixed {111} and {100} type planes, and elongates along the [110] direction. Based on a geometric calculation (Figure S2 in SI), plane (1$\bar{1}$1) intersects with plane (111) and (100) at line [$\bar{1}$01] and [011], respectively. These two lines (*i.e.*, [$\bar{1}$01] and [011]) intersect and form an angle of 60°, which matches with the interplane angles of the two ends of a typical Au nanorod (60°).

Graphic phase analysis (GPA) was carried out to further study the crystal properties of the synthesized Au nanorods. This technique enables one to measure lattice deformations based on a given HRTEM image.[39−41] Figure S3 in the SI shows the GPA study of an HRTEM image taken at the edge of an Au nanorod with the electron beam posed perpendicular to the rod's flat basal plane. Areas 1 and 2 were highlighted for the analysis in Figure S3A. Their relative positions as seen from the section view are schematically illustrated in the inset of Figure S3A. The strain image (ε_{xy}) (Figure S3B) shows distinct red and blue colors for areas 1 and 2, respectively. Taking area 1 as the reference (0%), a shear strain of −7% was measured in area 2. This shear strain arises from the phase difference,[41] defects, or different domain orientations between area 1 and 2.[40] Indeed, if viewed from the section view (inset of Figure S3A), area 1 corresponds to the twinning domain of T5, and area 2 corresponds to the overlapping of T4, T5, and T1. Since area 1 is positioned at the grain boundary of T4 and T5 (or T1 and T5), which sustains larger internal stress than the inner area of T4 (area 2),the strain of area 1 (0%) is larger than that of area 2 (−7%).

Synthesis and Characterization of Six-Star AuNPs. The synthesis of six-star AuNPs follows a seed-mediated sequential process (Scheme 1B). First, an ethanolic solution of $HAuCl_4$ (*ca.* 0.15 mM) and TiO_2 sol (*ca.* 33 mM) was photoirradiated at 80% of the lamp power for 40 min (step 1 in Scheme 1B). A 40 μL portion of this solution containing the seed NPs was mixed with a fresh 2 mL ethanolic solution containing $HAuCl_4$ (*ca.* 0.15 mM) and TiO_2 sol (*ca.* 33 mM) (step 2 in Scheme 1B). This mixed solution was then photoirradiated at 30% of the lamp power for 3 h to prepare the final products (step 3 in Scheme 1B). The obtained AuNP possesses a six-fold symmetry axis, with six branches protruding out, like a six-pointed-star (Figure 2), which is a platelet structure with a size of 250−350 nm (Figure 2A−C) and thicknesses of 60−80 nm (inset of Figure 2A). The selected area electron diffraction (SAED) pattern of a star lying on its basal plane shows the [111] zone reflections (Figure 2D). The pattern also reveals the forbidden 1/3{422} reflections, which are often observed in plates of Au or Ag having stacking or twinning planes normal to the electron beam.[21,42] HRTEM images were taken at the edge and tip portions of a star branch (Figure 2E,F, designated in Figure 2C), where the lattice spacings of 1.4 and 2.5 Å correspond to the {220} planes and 1/3{224} planes, respectively. Periodic stacking faults are shown at the tip portion of a star branch (Figure 1F) along one of the ⟨112⟩ directions with a Burgers vector of 1/2[110]. Similar defects are found at other branches, which partially explains the fast extension along the ⟨112⟩ directions and the formation of the six branches of an Au star. On the basis of the SAED pattern and the HRTEM images, a crystallographic model of the six-star AuNP is drawn in Figure 2G. The flat top and bottom planes of

a six-star AuNP are bound by the {111} type facets. The elongation of the star branches is along the six ⟨112⟩ directions, which gives a well-defined 6-fold symmetric 2-D architecture.

We also examined the Au seeds (Step 1 in Scheme 1B), used for preparing the six-star AuNPs, by TEM, which shows that the obtained pseudospherical Au seeds are about 35 nm in size (Figure S4 in SI). Internal defects and the SAED pattern of a typical Au seed suggest that they are not single crystals (inset in Figure S4 in the SI, some defects are marked in Figure S4). It is postulated that the internal strains of the seed AuNPs could be slowly relieved during the slow reduction process and the six-star AuNPs were obtained (recall that stacking faults are observed at the six branches, Figure 2F). In addition, when less seeds were used (4 μL seed solution in 2 mL fresh growth solution), the crystals grew into larger platelets with a size of *ca.* 1 μm and thickness of *ca.* 100 nm (Figure S5 in SI).

Role of TiO_2 in Photocatalytic Reactions. To investigate the role of TiO_2 sols in the photochemical synthesis, the UV−vis spectrum was used to monitor the process. Taking the photoirradiation of an ethanolic solution of $HAuCl_4$ (ca. 0.15 mM) and TiO_2 sol (*ca.* 33 mM) for example (Figure S6A in SI), before the photoirradiation ($t = 0$ min), the strong UV absorption before 350 nm and a shoulder at *ca.* 400 nm are attributed to the TiO_2 sols and $HAuCl_4$, respectively (UV−vis spectra of pure TiO_2 sols and $HAuCl_4$ in ethanol are shown in Figure S7 and S8, respectively, in SI). The solution color changes from light yellow to colorless during the first 10 min of reaction, indicated by the decreasing of the adsorption shoulder at *ca.* 400 nm (Figure S6A), which suggests the reduction of Au^{3+} in the solution started. When the reaction time increases, the intensity of the peak at *ca.* 550 nm, indicating the formation of AuNPs, increases gradually, accompanied with continuous red-shifting due to the enlargement of the NPs.

The photocatalytic reduction of $AgNO_3$ and $HAuCl_4$ on the excited TiO_2 and other semiconducting metal-oxide surfaces has been reported previously, and the reaction mechanisms have been studied intensively.[43−45] In this work, the colloidal TiO_2 prepared from the hydrolysis of titanium isopropoxide has a strong UV absorption before 350 nm (Figure S7 in SI), indicating the quantum size effect arising from the TiO_2 particles with size <5 nm.[44,45] This is in agreement with the size of TiO_2 particles used in our experiments, 1−3 nm measured by atomic force microscopy (AFM) (Figure 3A). In a typical photocatalytic reaction, electron and hole pairs are generated in the TiO_2 particles upon UV excitation (Figure S6B in SI and Reaction 1) ($E_{VB} \approx 2.7$ V *vs* SHE, $E_{CB} \approx -0.5$ V *vs* SHE, at pH 7).[44,46] The photogenerated electrons were transferred to and thus reduced the surrounding $AuCl_4^-$ ions (Reaction 2), while the holes were scavenged by the alcohols (Reactions 3 and 4).[34,35,44,46] Note that besides ethanol as the solvent,

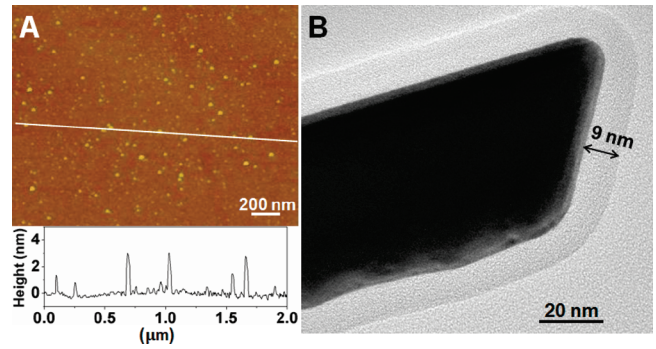

Figure 3. (A) AFM measurement of TiO_2 particles on a Si/SiO_2 substrate. (B) TEM image of the tip portion of a typical Au nanorod after being washed with ethanol once and dried in air. A layer of amorphous TiO_2 with the thickness of about 9 nm is observed, which is uniformly coated on the rod surface.

the TiO_2 solution contains a small amount of isopropyl alcohol, about 20 mM, coming from the hydrolysis of titanium isopropoxide.[35]

$$TiO_2 + h\nu \rightarrow TiO_2(h + e) \quad (1)$$

$$TiO_2(3e) + Au^{3+} \rightarrow TiO_2 + Au \quad (2)$$

$$TiO_2(2h) + C_2H_5OH \rightarrow TiO_2(e) + 2H^+ + CH_3CHO \quad (3)$$

$$TiO_2(2h) + (CH_3)_2CHOH \rightarrow TiO_2(e) + 2H^+ + (CH_3)_2CHO \quad (4)$$

As reported previously, $AuCl_4^-$ itself can be photochemically reduced to Au atoms.[33,47] To confirm the catalytic effect of TiO_2 sols in synthesizing AuNPs, control experiments were conducted by irradiation of 0.15 mM $HAuCl_4$ in ethanol or isopropyl alcohol for 2 h using 80% of the lamp full power without addition of any TiO_2. The solution color changed from light yellow to colorless, due to the photoinduced reduction of Au^{3+} to Au^+.[47] However, no AuNPs were obtained, confirmed by UV−vis spectrum (Figure S9 in SI). Therefore, TiO_2 sols are critical in catalyzing the reduction and nucleation of AuNPs.

Once the nucleation of AuNPs starts, the TiO_2 sol continues to catalyze the reaction, and the AuNPs also harvest the light energy through plasmonic excitation.[48] This is confirmed by illuminating a mixture of 1 mL of 35 nm Au seed solution, 4 mL of absolute ethanol, and 100 μL of 10 mM $HAuCl_4$ ethanolic solution for 4 h (the Au seeds were washed with ethanol four times to remove the residual TiO_2). A 500 nm band-pass filter was used to block the UV region of the light source. Before the reaction begins, the solution has an absorption peak at 323 nm and a shoulder at *ca.* 400 nm for $HAuCl_4$, and another peak positioned at *ca.* 556 nm for the Au seeds (Figure S10 in SI). After 4 h of excitation, the intensity of the peak at 323 nm significantly decreased, and the 556 nm peak red-shifted to *ca.* 610 nm accompanied by twice the increase in the intensity, due to the enlargement of the Au seeds. This

proves that the visible-light excited Au seeds can catalyze the reduction of $HAuCl_4$, resulting in the continuous deposition of Au atoms onto the existing Au particle surfaces to form enlarged Au particles.

Besides the catalytic role, the TiO_2 particles have also acted as the stabilizing/capping agent during the synthesis of Au nanocrystals (AuNCs). In previous reports, the colloidal metal-oxides have been used to stabilize metal NPs through electrostatic interactions.[49,50] Since the isoelectric point of TiO_2 is *ca.* 5,[51−53] in our experiment, the TiO_2 particles are positively charged in the acidic condition, indicated by the zeta potential of +27.8 mV measured in the as-prepared 33 mM TiO_2 sols (at pH 2). The interaction between $AuCl_4^-$ and the positively charged TiO_2 favors the binding of TiO_2 particles onto the surface of the AuNCs. Evidently, about 9 nm thick of TiO_2 is found uniformly covered on the surface of a typical Au nanorod, which was only washed by ethanol once and dried in air (Figure 3B). The component of the coating layer was confirmed by the energy dispersive X-ray spectroscopy (EDS) analysis, which shows the elements of O, Ti, and Au (Figure S11 in SI. Note that the signal of Au is also showing up because of the limited resolution of the EDS detector). The TiO_2 layer gave no SAED pattern, suggesting it is amorphous. It can be postulated that during the synthesis, the 1−3 nm TiO_2 particles interact and stabilize the growing AuNPs through the electrostatic interaction, which was previously observed in the TiO_2 nanorod-assisted synthesis of spherical AgNPs.[49] In our purification process, the Au nanorods need to be washed with ethanol for at least three times to remove the TiO_2 particles. Hence, when the rods are only washed once and then dried in air, the high density of TiO_2 sol particles, initially absorbed on the rod surface, will collide and condense to gels and eventually result in a layer of amorphous TiO_2 covering the Au rod surface.[54] Importantly, because the TiO_2 particles are so small (1−3 nm) and disperse well in the synthesis solution, they are effective in stabilizing the synthesized AuNPs without the addition of any other capping agents.

pH Effect. Since HCl was added during the hydrolysis of titanium isopropoxide to prepare the small sized TiO_2 sol particles,[44,45,54] our subsequent syntheses of the AuNCs were carried out in acidic conditions. The as-prepared TiO_2 sols (33 mM), and 16-times diluted sols (2.1 mM) are at pH 2 and 3.5, respectively. When the pH of the as-prepared sols was adjusted by the addition of NaOH to *ca.* 5, close to the isoelectric point of TiO_2, the transparent colloidal solution turned milky white, indicating the agglomeration of the small TiO_2 particles.[54] A direct influence of the acidic environment on our synthesis is the oxidative etching of AuNCs during the synthesis, evidenced by the fact that the obtained Au nanorods and six-star AuNPs do not exhibit sharp but slightly rounded tips (Figure 1 and 2). In addition, to investigate the effect of acidity on the product morphology, we added additional HCl to the growth solution for the nanorods, from the original 0.25 mM to 10 mM. Longer platelet-like nanorods were obtained, with length of 4.3 ± 0.7 μm (Figure S12 in SI). However, it took longer time, about 3 h, to complete the reaction, because the increased acidity suppressed the reduction of Au^{3+} ions.[55]

Shape control of Au nanocrystals (AuNCs). Besides the platelet-like nanorods and the six-star AuNPs, we have also synthesized Au triangular prisms and branched AuNPs (Figure S13, Table S1 in SI). The morphology of the AuNCs was controlled by tuning the concentrations of $HAuCl_4$ and TiO_2, or through a seeding procedure. As mentioned above, the six-star AuNPs could only be prepared in a seeding method in our experiments. For other syntheses without a seeding process, when the concentration ratio of $TiO_2/HAuCl_4$ increased, different morphologies of AuNCs were obtained, that is, from platelet-like nanorods, triangular prisms, to branched NPs (Table S1 in SI).

On the basis of the previous investigations, the intrinsic properties of the NPs (or seeds) formed at the very early stage, that is, the absence or presence of crystal defects (stacking faults and twins), partially determine the morphologies of the final structures.[18−21] In the thermodynamic controlled synthesis, the nucleation of noble metals usually gives rise to mixed seeds of single crystals, singly twinned, and multiply twined structures such as pentagons and icosahedrons.[20] Other seed structures with stacking faults are frequently observed in kinetic controlled processes, such as in mild reducing environment where insufficient atoms are available for the minimization of surface energy.[20]

One of the most direct means to slow down a reaction in the wet chemical synthesis is to use a mild reducing agent, while in the photochemical synthesis, particularly in our TiO_2-catalyzed synthesis, decreasing the power of the light source can directly hinder the reducing ability of the growth solution. Therefore, a halogen lamp with tunable intensity was used in our experiment, that is, the seeding process to prepare the six-star AuNPs. As mentioned above, we used 80% and 30% of the lamp power to synthesize the defected seeds and to further develop the structures, respectively (Scheme 1B). To further elucidate the effect of light power on the growth rate of Au nanostructures, we examined the products at different growth stages during the synthesis of the six-star AuNPs. The seeds used in this process as mentioned before were ∼35 nm AuNPs (Figure S14A in SI). After they were photoirradiated in a fresh growth solution for 45 min, they grew larger with an average size of ∼65 nm, and some of them began to show extending branches as indicated by the red arrows in one NP (Figure S14B in SI). After 2 more hours of slow growth, the branches became more regular as the NPs grew larger, and finally six-star NPs were obtained (Figure S14C in SI). For comparison, if 80%, instead of 30%, of the lamp power was used to irradiate the seed NPs in a fresh growth solution for 45 min, the seed NPs grew into very irregularly shaped NPs with sizes up to 100 nm (Figure S14D in SI). Among these

big NPs, some smaller sized NPs (size of ~40 nm) were present as well, which probably were not from the enlargement of the ~35 nm seed NPs, but were newly formed because the relatively higher power (80% of intensity) was used. Therefore, in our synthesis method, it is critical that during the subsequent growth, the mild reducing environment (30% of lamp power) and longer reaction time (*ca.* 3 h) should be provided to synthesize the well-defined six-star AuNPs.

CONCLUSION

We present the shape-controlled synthesis of anisotropic Au nanocrystals (AuNCs) by photoirradiation of the mixture of TiO_2 sols and $HAuCl_4$ in ethanol. By changing the concentrations of TiO_2 and $HAuCl_4$ and using a seeding procedure, AuNCs with different morphologies can be obtained, which include two unique structures, that is, the platelet-like Au nanorods and the six-star AuNPs. Importantly, the platelet-like rods are the asymmetric 5-fold twinned structures. In addition, the colloidal TiO_2 acts as the photocatalyst as well as the stabilizing agent for the synthesized AuNCs. We have also demonstrated that in such photochemical synthesis, the ability to manipulate light intensity allows one to adjust the light power for the photochemical reaction and kinetically control the crystal evolution at different stages. Our method might be extended to shape-controlled photochemical synthesis of other metallic nanostructures.

MATERIAL AND METHODS

Chemicals. Titanium isopropoxide (99.999%, Sigma-Aldrich, Milwaukee, WI, USA), hydrogen chloride (fuming, 37%, Merck, Germany), ethanol (99.9%, absolute, Merck, Germany), isopropyl alcohol (HPLC grade, Fisher, Singapore), and hydrogen tetrachloroaurate (III) (ACS, 99.99%, Alfa Aesar, USA) were used without further purification. Ultrapure Milli-Q water (Milli-Q System, Millipore, Billerica, MA, USA) was used in all experiments.

Preparation of TiO_2 Sol. All glassware was washed with Aqua Regia, $HCl:HNO_3$ = 3:1 (v:v), and rinsed with ethanol and Milli-Q water (**CAUTION**: Aqua Regia is a very corrosive oxidizing agent, which should be handled with great care). Colloidal TiO_2 was prepared as follows: 0.4 mL of 0.2 mM HCl was diluted in 18 mL of ethanol (solution **1**); 0.2 mL of titanium-tetraisopropoxide was dissolved in 1.9 mL of ethanol (solution **2**). After solution **2** was added slowly dropwise to solution **1** with vigorous stirring at 0 °C, the mixed solution was further stirred for 5 h to give a transparent TiO_2 sol, with concentration of *ca.* 33 mM.

Photochemical Synthesis of Platelet-like Au Nanorods. The as-prepared 33 mM TiO_2 sol was diluted 16 times with absolute ethanol to be used for the synthesis of platelet-like Au nanorods. A 2 mL portion of ethanolic solution of $HAuCl_4$ (*ca.* 0.2 mM) and TiO_2 sol (*ca.* 2.1 mM) in a 3 mL capped quartz reactor was photoirradiated with a 150 W quartz halogen fiber optic illuminator (mode MI-150, Fiber-Lite, USA), at 80% of the lamp power for 2 h. The reactor was placed 2 cm away from the light source. It was monitored that the temperature of the solution increased to about 35 °C during the reaction.

Photochemical Synthesis of Six-Star AuNPs. One milliliter of ethanolic solution of $HAuCl_4$ (*ca.* 0.15 mM) and TiO_2 sol (*ca.* 33 mM) was photoirradiated at 80% of the lamp power. A UV spectrophotometer (UV-1800, Shimadzu, Japan) was used to monitor the evolution of AuNPs during the photoirradiation process. After 40-min photoirradiation, the reaction was stopped (step 1 in Scheme 1B), and the solution was used as a seed solution. A 40 μL portion of this seed solution was mixed with 2 mL of ethanolic solution of $HAuCl_4$ (*ca.* 0.15 mM) and TiO_2 sol (*ca.* 33 mM) (step 2 in Scheme 1B), and then this mixture was slowly irradiated at 30% of the lamp power for 3 h (step 3 in Scheme 1B). The final solution was centrifuged and washed with ethanol for three times and then washed with and redispersed in Milli-Q water.

Characterizations. A drop of the solution containing Au nanomaterials was placed on silicon, glass, and holey carbon-coated copper grid, and naturally dried in air prior to characterization by field-emission scanning electron microscopy (FE-SEM, JSM-6340F, Japan), X-ray diffraction analysis (XRD, Rigaku, Japan), and transmission electron microscopy (TEM, JEM-2010F, Japan), respectively. FE-SEM, XRD, and TEM were performed at 5 keV in the secondary electron mode, theta/2-theta mode with the scan rate of 0.1°/min and 200 kV, respectively.

Acknowledgment. The authors acknowledge financial support from AcRF Tier 1 (RG 20/07) and AcRF Tier 2 from MOE, CRP (NRF-CRP2-2007-01) from NRF, A*STAR SERC Grant (No. 092 101 0064) and the Centre for Biomimetic Sensor Science at NTU in Singapore. C.X. acknowledges the support of Start-Up Grant (SUG, LKY 4/08) from NTU for the Lee Kuan Yew Research Fellowship, CRP (NRF-CRP5-2009-04) from NRF, and the Centre for Artificial Photosynthesis System (CAPS) at NTU in Singapore.

Supporting Information Available: The SEM, TEM images, XRD data, EDS spectrum, GPA data, UV−vis spectra and Table for different morphologies of the synthesized of Au nanostructures. This material is available free of charge *via* the Internet at http://pubs.acs.org.

REFERENCES AND NOTES

1. Narayanan, R.; El-Sayed, M. A. Catalysis with Transition Metal Nanoparticles in Colloidal Solution: Nanoparticle Shape Dependence and Stability. *J. Phys. Chem. B* **2005**, *109*, 12663–12676.
2. Hutter, E.; Fendler, J. H. Exploitation of Localized Surface Plasmon Resonance. *Adv. Mater.* **2004**, *16*, 1685–1706.
3. Mirkin, C. A.; Letsinger, R. L.; Mucic, R. C.; Storhoff, J. J. A DNA-Based Method for Rationally Assembling Nanoparticles into Macroscopic Materials. *Nature* **1996**, *382*, 607–609.
4. Link, S.; El-Sayed, M. A. Shape and Size Dependence of Radiative, Non-radiative and Photothermal Properties of Gold Nanocrystals. *Int. Rev. Phys. Chem.* **2000**, *19*, 409–453.
5. Sanchez-Iglesias, A.; Pastoriza-Santos, I.; Perez-Juste, J.; Rodriguez-Gonzalez, B.; de Abajo, F. J. G.; Liz-Marzan, L. M. Synthesis and Optical Properties of Gold Nanodecahedra with Size Control. *Adv. Mater.* **2006**, *18*, 2529–2534.
6. Sau, T. K.; Murphy, C. J. Room Temperature, High-Yield Synthesis of Multiple Shapes of Gold Nanoparticles in Aqueous Solution. *J. Am. Chem. Soc.* **2006**, *126*, 8648–8649.
7. Tréguer-Delapierre, M.; Majimel, J.; Mornet, S.; Duguet, E.; Ravaine, S. Synthesis of Non-spherical Gold Nanoparticles. *Gold Bull.* **2008**, *41*, 195–207.
8. Zhang, J.; Liu, H.; Wang, Z.; Ming, N. Shape-Selective Synthesis of Gold Nanoparticles with Controlled Sizes, Shapes, and Plasmon Resonances. *Adv. Funct. Mater.* **2007**, *17*, 3295–3303.
9. Chen, S. H.; Wang, Z. L.; Ballato, J.; Foulger, S. H.; Carroll, D. L. Monopod, Bipod, Tripod, and Tetrapod Gold Nanocrystals. *J. Am. Chem. Soc.* **2003**, *125*, 16186–16187.
10. Yamamoto, M.; Kashiwagi, Y.; Sakata, T.; Mori, H.; Nakamoto, M. Synthesis and Morphology of Star-Shaped Gold Nanoplates Protected by Poly(*N*-vinyl-2-pyrrolidone). *Chem. Mater.* **2005**, *17*, 5391–5393.
11. Zhang, J.; Du, J.; Han, B.; Liu, Z.; Jiang, T.; Zhang, Z. Sonochemical Formation of Single-Crystalline Gold Nanobelts. *Angew. Chem., Int. Ed.* **2006**, *45*, 1116–1119.
12. Xu, X.; Cortie, M. B. Shape Change and Color Gamut in Gold Nanorods, Dumbbells, and Dog Bones. *Adv. Funct. Mater.* **2006**, *16*, 2170–2176.

13. Johnson, C. J.; Erik, D.; Davis, S. A.; Murphy, C. J.; Mann, S. Growth and Form of Gold Nanorods Prepared by Seed-Mediated, Surfactant-Directed Synthesis. *J. Mater. Chem.* **2002**, *12*, 1765–1770.
14. Murphy, C. J. Anisotropic Metal Nanoparticles: Synthesis, Assembly, and Optical Applications. *J. Phy. Chem. B* **2005**, *109*, 13857–13870.
15. Huang, X. H.; El-Sayed, I. H.; Qian, W.; El-Sayed, M. A. Cancer Cell Imaging and Photothermal Therapy in the Near-Infrared Region by Using Gold Nanorods. *J. Am. Chem. Soc.* **2006**, *128*, 2115–2120.
16. Seo, D.; Park, J. C.; Song, H. Polyhedral Gold Nanocrystals with O_h Symmetry: From Octahedra to Cubes. *J. Am. Chem. Soc.* **2006**, *128*, 14863–14870.
17. Millstone, J. E.; Wei, W.; Jones, M. R.; Yoo, H.; Mirkin, C. A. Iodide Ions Control Seed-Mediated Growth of Anisotropic Gold Nanoparticles. *Nano Lett.* **2008**, *8*, 2526–2529.
18. Grzelczak, M.; Perez-Juste, J.; Mulvaney, P.; Liz-Marzan, L. M. Shape Control in Gold Nanoparticle Synthesis. *Chem. Soc. Rev.* **2008**, *37*, 1783–1791.
19. Tao, A. R.; Habas, S.; Yang, P. D. Shape Control of Colloidal Metal Nanocrystals. *Small* **2008**, *4*, 310–325.
20. Xia, Y.; Xiong, Y.; Lim, B.; Skrabalak, S. E. Shape-Controlled Synthesis of Metal Nanocrystals: Simple Chemistry Meets Complex Physics? *Angew. Chem., Int. Ed.* **2008**, *47*, 2−46.
21. Lofton, C.; Sigmund, W. Mechanisms Controlling Crystal Habits of Gold and Silver Colloids. *Adv. Funct. Mater.* **2005**, *15*, 1197–1208.
22. Liu, X.; Wu, N.; Wunsch, B. H.; Barsotti, R. J., Jr.; Stellacci, F. Shape-Controlled Growth of Micrometer-Sized Gold Crystals by a Slow Reduction Method. *Small* **2006**, *2*, 1046–1050.
23. Martin, C. R. Membrane-Based Synthesis of Nanomaterials. *Chem. Mater.* **1996**, *8*, 1739–1746.
24. Yin, Z. Y.; Wu, S. X.; Zhou, X. Z.; Huang, X.; Zhang, Q. C.; Boey, F.; Zhang, H. Electrochemical Deposition of ZnO Nanorods on Transparent Reduced Graphene Oxide Electrodes for Hybrid Solar Cells. *Small* **2010**, *6*, 307–312.
25. Wu, S. X.; Yin, Z. Y.; He, Q. Y.; Huang, X.; Zhou, X. Z.; Zhang, H. Electrochemical Deposition of Semiconductor Oxides on Reduced Graphene Oxide-Based Flexible, Transparent and Conductive Electrodes. *J. Phys. Chem. C.* **2010**, *114*, 11816–11821.
26. Kim, F.; Song, J. H.; Yang, P. Photochemical Synthesis of Gold Nanorods. *J. Am. Chem. Soc.* **2002**, *124*, 14316–14317.
27. Lu, X. M.; Yavuz, M. S.; Tuan, H. Y.; Korgel, B. A.; Xia, Y. N. Ultrathin Gold Nanowires Can Be Obtained by Reducing Polymeric Strands of Oleylamine AuCl Complexes Formed *via* Aurophilic Interaction. *J. Am. Chem. Soc.* **2008**, *130*, 8900–8901.
28. Wang, C.; Hu, Y. J.; Lieber, C. M.; Sun, S. H. Ultrathin Au Nanowires and Their Transport Properties. *J. Am. Chem. Soc.* **2008**, *130*, 8902–8903.
29. Huo, Z. Y.; Tsung, C. K.; Huang, W. Y.; Zhang, X. F.; Yang, P. D. Sub-Two Nanometer Single Crystal Au Nanowires. *Nano Lett.* **2008**, *8*, 2041–2044.
30. Jasuja, K.; Vikas, B. Implantation and Growth of Dendritic Gold Nanostructures on Graphene Derivatives: Electrical Property Tailoring and Raman Enhancement. *ACS Nano* **2009**, *3*, 2358–2366.
31. Dahl, J. A.; Maddux, B. S.; Hutchison, J. E. Toward Greener Nanosynthesis. *Chem. Rev.* **2007**, *107*, 2228–2269.
32. Zhu, J. M.; Shen, Y. H.; Xie, A. J.; Qiu, L. G.; Zhang, Q.; Zhang, S. Y. Photoinduced Synthesis of Anisotropic Gold Nanoparticles in Room-Temperature Ionic Liquid. *J. Phys. Chem. C* **2007**, *111*, 7629–7633.
33. Eustis, S.; Hsu, H. Y.; El-Sayed, M. A. Gold Nanoparticle Formation from Photochemical Reduction of Au^{3+} by Continuous Excitation in Colloidal Solutions. A Proposed Molecular Mechanism. *J. Phys. Chem. B* **2005**, *109*, 4811–4815.
34. Wang, C.-Y.; Liu, C.-Y.; Zheng, X.; Chen, J.; Shen, T. The Surface Chemistry of Hybrid Nanometer-Sized Particles II. Characterization and Microstructure of Au Clusters Supported on TiO_2. *J. Colloid Interface Sci.* **1997**, *191*, 464–470.
35. Wang, C.-Y.; Liu, C.-Y.; Zheng, X.; Chen, J.; Shen, T. The Surface Chemistry of Hybrid Nanometer-Sized Particles I. Photochemical Deposition of Gold on Ultrafine TiO_2 Particles. *Colloid Surf. A* **1998**, *131*, 271–280.
36. Huang, X.; Zhou, X. Z.; Wu, S. X.; Wei, Y. Y.; Qi, X. Y.; Zhang, J.; Boey, F.; Zhang, H. Reduced Graphene Oxide-Templated Photochemical Synthesis and *in Situ* Assembly of Au Nanodots to Orderly Patterned Au Nanodot Chains. *Small* **2010**, *6*, 513–516.
37. Gryaznov, V. G.; Heydenreich, J.; Kaprelov, A. M.; Nepijko, S. A.; Romanov, A. E.; Urban, J. Pentagonal Symmetry and Disclinations in Small Particles. *Cryst. Res. Technol* **1999**, *34*, 1091–1119.
38. Marks, L. D.; Ajayan, P. M. Quasi-melting of Small Particles. *Ultramicroscopy* **1986**, *20*, 77–82.
39. Hÿtch, M. J.; Snoeck, E.; Kilaas, R. Quantitative Measurement of Displacement and Strain Fields from HREM Micrographs. *Ultramicroscopy* **1998**, *74*, 131–146.
40. Johnson, C. L.; Snoeck, E.; Ezcurdia, M.; Rodriguez-Gonzalez, B.; Pastoriza-Santos, I.; Liz-Marzan, L. M.; Hytch, M. J. Effects of Elastic Anisotropy on Strain Distributions in Decahedral Gold Nanoparticles. *Nat. Mater.* **2008**, *7*, 120–124.
41. Tirry, W.; Schryvers, D. Linking a Completely Three-Dimensional Nanostrain to a Structural Transformation Eigenstrain. *Nature* **2009**, *8*, 752–757.
42. Sun, Y.; Mayers, B.; Xia, Y. Transformation of Silver Nanospheres into Nanobelts and Triangular Nanoplates through a Thermal Process. *Nano Lett.* **2003**, *3*, 675–679.
43. Choi, W.; Hoffmann, M. R. Photoreductive Mechanism of CCl_4 Degradation on TiO_2 Particles and Effects of Electron Donors. *Environ. Sci. Technol.* **1995**, *29*, 1646–1654.
44. Kamat, P. V.; Bedja, I.; Hotchandani, S. Photoinduced Charge Transfer between Carbon and Semiconductor Clusters. One-Electron Eduction of C_{60} in Colloidal TiO_2 Semiconductor Suspensions. *J. Phys. Chem.* **1994**, *98*, 9137–9142.
45. Kamat, P. V. Photochemistry on Nonreactive and Reactive (Semiconductor) Surfaces. *Chem. Rev.* **1993**, *93*, 267–270.
46. Willianms, G.; Seger, B.; Kamat, P. V. TiO_2−Graphene Nanocomposites. UV-Assisted Photocatalytic Reduction of Graphene Oxide. *ACS Nano* **2008**, *2*, 1487–1491.
47. Kurihara, K.; Kizling, J; Stenius, P; Fendler, J. H. Laser and Pulse Radiolytically Induced Colloidal Gold Formation in Water and in Water-in-Oil Microemulsions. *J. Am. Chem. Soc.* **1983**, *105*, 2574–2579.
48. Xue, C.; Millstone, J. E.; Li, S.; Mirkin, C. A. Plasmon-Driven Synthesis of Triangular Core−Shell Nanoprisms from Gold Seeds. *Angew. Chem., Int. Ed.* **2007**, *46*, 8436–8439.
49. Cozzoli, P. D.; Comparelli, R.; Fanizza, E.; Curri, M. L.; Agostiano, A.; Laub, D. Photocatalytic Synthesis of Silver Nanoparticles Stabilized by TiO_2 Nanorods: A Semiconductor/Metal Nanocomposite in Homogeneous Nonpolar Solution. *J. Am. Chem. Soc.* **2004**, *126*, 3868–3879.
50. Subramanian, V.; Wolf, E. E.; Kamat, P. V. Green Emission to Probe Photoinduced Charging Events in ZnO−Au Nanoparticles. Charge Distribution and Fermi-Level Equilibration. *J. Phys. Chem. B* **2003**, *107*, 7479–7458.
51. Imhof, A. Preparation and Characterization of Titania-Coated Polystyrene Spheres and Hollow Titania Shells. *Langmuir* **2001**, *17*, 3579–3585.
52. Chen, X.; Cheng, H.; Ma, J. A Study on the Stability and Rheological Behavior of Concentrated TiO_2 Dispersions. *Powder Technol.* **1998**, *99*, 171–176.
53. Joseph, W. B.; Cima, M. J. Orientation Dependence of the Isoelectric Point of TiO_2 (Rutile) Surfaces. *Langmuir* **2006**, *22*, 10264–10271.
54. Hench, L. L.; West, J. K. The Sol−Gel Process. *Chem. Rev.* **1990**, *90*, 33–72.
55. Kim, F.; Sohn, K.; Wu, J.; Huang, J. Chemical Synthesis of Gold Nanowires in Acidic Solutions. *J. Am. Chem. Soc.* **2008**, *130*, 14442–14443.